



Contents lists available at ScienceDirect

Metabolic Engineering Communications

journal homepage: www.elsevier.com/locate/mec

Improving designer glycan production in *Escherichia coli* through model-guided metabolic engineering

Joseph A. Wayman^a, Cameron Glasscock^b, Thomas J. Mansell^b, Matthew P. DeLisa^b,
Jeffrey D. Varner^{b,*}

^a School of Applied and Engineering Physics, Cornell University, Ithaca, NY, 14853, USA

^b Robert Frederick Smith School of Chemical and Biomolecular Engineering, Cornell University, Ithaca, NY, 14853, USA



ARTICLE INFO

Keywords:

Glycosylation
Metabolic modeling
Microbial glycobiology
N-linked glycan
Strain engineering

ABSTRACT

Asparagine-linked (N-linked) glycosylation is the most common protein modification in eukaryotes, affecting over two-thirds of the proteome. Glycosylation is also critical to the pharmacokinetic activity and immunogenicity of many therapeutic proteins currently produced in complex eukaryotic hosts. The discovery of a protein glycosylation pathway in the pathogen *Campylobacter jejuni* and its subsequent transfer into laboratory strains of *Escherichia coli* has spurred great interest in glycoprotein production in prokaryotes. However, prokaryotic glycoprotein production has several drawbacks, including insufficient availability of non-native glycan precursors. To address this limitation, we used a constraint-based model of *E. coli* metabolism in combination with heuristic optimization to design gene knockout strains that overproduced glycan precursors. First, we incorporated reactions associated with *C. jejuni* glycan assembly into a genome-scale model of *E. coli* metabolism. We then identified gene knockout strains that coupled optimal growth to glycan synthesis. Simulations suggested that these growth-coupled glycan overproducing strains had metabolic imbalances that rerouted flux toward glycan precursor synthesis. We then validated the model-identified knockout strains experimentally by measuring glycan expression using a flow cytometric-based assay involving fluorescent labeling of cell surface-displayed glycans. Overall, this study demonstrates the promising role that metabolic modeling can play in optimizing the performance of a next-generation microbial glycosylation platform.

1. Introduction

Protein glycosylation is the attachment of glycans (mono-, oligo-, or polysaccharide) to specific amino acid residues in proteins, most commonly asparagine (N-linked) or serine and threonine (O-linked) residues. Roughly three-quarters of eukaryotic proteins and more than half of prokaryotic proteins are glycosylated (Dell et al., 2010). Glycosylation is also vitally important to the development of many protein biologics, and has been harnessed for enhancing therapeutic properties such as half-life extension (Elliott et al., 2003; Flintegaard et al., 2010; Ilyushin et al., 2013; Lindhout et al., 2011), antibody-mediated cytotoxicity (Li et al., 2017; Lin et al., 2015), and immunogenicity (Lipinski et al., 2013; Sadoulet et al., 2007; Wacker et al., 2014).

Though once thought to occur only in eukaryotes, protein glycosylation has now been discovered in all three domains of life, including bacteria (Nothaft and Szymanski, 2010). The best characterized bacterial N-glycosylation system is that of the human pathogen *Campylobacter*

jejuni (Szymanski et al., 1999). The *C. jejuni* glycan has the form of a branched heptasaccharide Glc GalNAc₅ Bac, where Glc is glucose, GalNAc is N-acetylgalactosamine, and Bac is bacillosamine. This glycan is assembled on the lipid carrier undecaprenyl pyrophosphate (Und-PP) on the cytoplasmic face of the inner membrane by an enzymatic pathway encoded by the *pgl* (protein glycosylation) locus (Fig. 1). The fully assembled glycan is flipped across the membrane and transferred to asparagine residues in acceptor proteins by the oligosaccharyltransferase (OST) PglB. PglB attaches the heptasaccharide to periplasmically-localized proteins containing the consensus sequence D/E-X-N-Z-S/T, where X and Z are any residue except proline (Fisher et al., 2011; Kowarik et al., 2006).

The functional transfer of this system into *E. coli* (Wacker et al., 2002) has spurred interest in recombinant production of glycans and ultimately therapeutic glycoproteins in this genetically tractable bacterial host (Merritt et al., 2013; Baker et al., 2013). Along these lines, glycosylation-competent *E. coli* cells have been used to produce a variety

* Corresponding author.

E-mail address: jdv27@cornell.edu (J.D. Varner).

<https://doi.org/10.1016/j.mec.2019.e00088>

Received 7 July 2017; Received in revised form 13 March 2019; Accepted 14 March 2019

2214-0301/© 2019 The Authors. Published by Elsevier B.V. on behalf of International Metabolic Engineering Society. This is an open access article under the CC BY-

NC-ND license (<http://creativecommons.org/licenses/by-nc-nd/4.0/>).

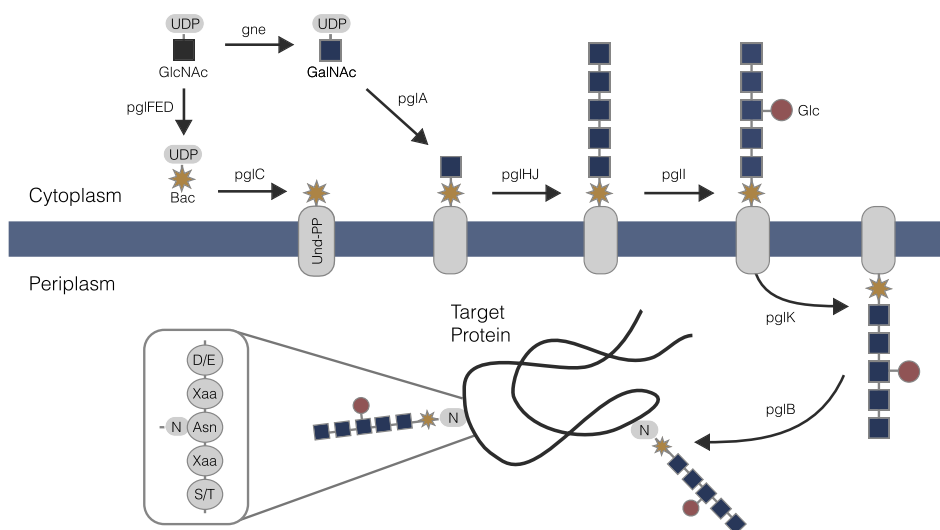


Fig. 1. Glycosylation pathway in *C. jejuni* and *E. coli*. Glycan assembly, facilitated by *pgl* locus enzymes, takes place on a lipid carrier, undecaprenyl pyrophosphate (Und-PP), from cytoplasmic pools of nucleotide-activated sugars N-acetylglucosamine (GlcNAc), N-acetylgalactosamine (GalNAc), and glucose (Glc). The glycan is then flipped onto the periplasmic side of the inner membrane, where it is transferred to an asparagine residue on a glycoprotein acceptor motif.

of periplasmic and extracellular glycoproteins including antibodies (Fisher et al., 2011) and conjugate vaccine candidates (Feldman et al., 2005). The promiscuity of the PglB enzyme towards structurally diverse lipid-linked glycan substrates has been exploited to further expand the *E. coli* platform, enabling the creation of glycoproteins bearing different bacterial O-polysaccharide antigens (Feldman et al., 2005; Ihssen et al., 2010) and even the eukaryotic trimannosyl core N-glycan produced by a synthetic pathway comprised of four yeast glycosyltransferases (Valderrama-Rincon et al., 2012). However, while PglB can efficiently glycosylate native *C. jejuni* acceptor proteins with cognate Glc GalNAc₅ Bac glycan in engineered *E. coli*, glycosylation of non-Campylobacter target proteins is often much less efficient (Schwarz et al., 2010), especially in combination with heterologous glycan structures (Valderrama-Rincon et al., 2012).

In engineered *E. coli*, protein glycosylation is affected by the availability of lipid carriers, and the availability of nucleotide-activated sugar substrates serving as glycan precursors (Merritt et al., 2013; Jaffé et al., 2014). Hence, a plausible strategy for increasing glycosylation efficiency is to optimize the levels of these key reaction intermediates and their related biosynthetic pathways. Along these lines, Wright and coworkers applied genome-scale metabolic engineering techniques to improve glycosylation efficiency in *E. coli*. Using a high-throughput proteomic screening and probabilistic metabolic network analysis, they showed that upregulation of the glyoxylate cycle by overexpression of isocitrate lyase (*aceA/icl*) increased glycosylation efficiency of a prototypic protein by three-fold (Pandhal et al., 2011). Further, genome-wide screening of gene overexpression identified targets that increased glycoprotein production as well as glycosylation efficiency (Pandhal et al., 2013); genes in pathways associated with glycan precursor synthesis (UDP-GlcNAc) as well as lipid carrier production (isoprenoid synthesis) were identified as bottlenecks. Improved glycosylation efficiency has also been achieved by supplementing growth media with GlcNAc (Kämpf et al., 2015) or increasing the expression of PglB via codon optimization (Pandhal et al., 2012). These studies and others have demonstrated the complex interplay between recombinant protein production, glycan synthesis and assembly, and glycosylation efficiency.

In this study, we addressed one of the challenges facing high-level glycoprotein production in engineered *E. coli*, namely the availability of glycan precursors, using constraint-based modeling. In particular, we used a constraint-based model of *E. coli* metabolism, in combination with heuristic optimization, to design gene knockout strains that overproduced glycan precursors. First, we incorporated reactions associated

with *C. jejuni* glycan assembly into a genome-scale model of *E. coli* metabolism. We then used a combination of constraint-based modeling and simulated annealing to identify gene knockout strains that coupled optimal growth to glycan synthesis. Simulations suggested that these growth-coupled glycan overproducing strains had metabolic imbalances that rerouted flux toward glycan precursor synthesis. We then experimentally validated the model-identified metabolic designs using a flow cytometric-based assay for quantifying cellular N-glycans in *E. coli* (Valderrama-Rincon et al., 2012). Consistent with simulations, the best model-predicted changes increased glycan production by nearly 3-fold compared with the glycan production level in wild-type (wt) *E. coli* cells. Taken together, our results reveal the significant impact that metabolic modeling can have on designing chassis strains with enhanced N-linked protein glycosylation capabilities.

2. Results

2.1. Construction of a constraint-based model of N-linked glycosylation in *E. coli*

A constraint-based model of N-glycosylation in *E. coli* was used to identify genetic knockouts that coupled glycan biosynthesis with optimal growth. We augmented the existing genome-scale *E. coli* model iAF1260 from Palsson and coworkers (Feist et al., 2007) to include the reactions of the *C. jejuni* glycosylation pathway (Table 1). The adapted network consisted of 2395 reactions, 1271 open reading frames, and 1986 metabolites segregated into cytoplasmic, periplasmic, and extracellular compartments. Added reactions included the biochemical transformations catalyzed by the glycosyltransferases (e.g., PglA, PglC) associated with glycan biosynthesis, PglK flippase-mediated translocation of the glycan into the periplasm, and PglB-mediated glycan conjugation to an acceptor protein (Fig. 1). In addition, we incorporated the transcriptional regulatory network of Covert et al., consisting of 101 transcription factors, regulating the state of the metabolic genes (Covert et al., 2004). This regulatory network imparts Boolean constraints on metabolic fluxes based upon the nutrient environment. The model code is available for download under an MIT software license from the Varnerlab website (<http://www.varnerlab.org/>).

2.2. Identification of growth-coupled gene knockout strains

To identify genetic knockouts that coupled optimal growth to glycan

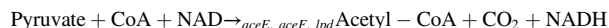
Table 1

Reactions added to the *E. coli* model iAF1260 (Feist et al., 2007) for biosynthesis of *C. jejuni* glycan. Species localized to the periplasm are denoted by (p), all others are cytoplasmic. Abbreviations: UDP-N-Acetyl-D-Glucosamine, UDP-GlcNAc; UDP-N-Acetyl-D-Galactosamine, UDP-GalNAc; UDP-2-acetamido-2,6-dideoxy- α -D-xylo-4-hexulose, KetoBac; L-Glutamate, Glu; UDP-N-Acetyl-bacillosamine, AminoBac; α -ketoglutarate, α KG; Acetyl-CoA, ACCoA; UDP-N,N'-diacetyl-bacillosamine, uBac; Coenzyme A, CoA; Undecaprenyl phosphate, Udcpp; *C. jejuni* glycan intermediates, UdcCjGlycan1, UdcCjGlycan6; Uridine monophosphate, UMP; Uridine diphosphate, UDP; UDP-Glucose, UDP-Glc; Lipid-linked *C. jejuni* glycan, UdcCjGlycan; Acceptor protein, AcceptorProt; GlycoProt, Glycoprotein; Undecaprenyl diphosphate, Udcppd.

Gene	Enzyme	Reaction	Reference
gne	UDP-GlcNAc epimerase	UDP-GlcNAc \rightarrow UDP-GalNAc	Bernatchez et al. (2005)
pglF	UDP-GlcNAc dehydratase	UDP-GlcNAc \rightarrow KetoBac + H ₂ O	Schoenhofen et al. (2006)
pglE	Aminotransferase	KetoBac + Glu \leftrightarrow AminoBac + α KG	Schoenhofen et al. (2006)
pglD	Acetyltransferase	AminoBac + ACCoA \rightarrow uBac + CoA + H ⁺	Olivier et al. (2006)
pglC	Bacillosamine transferase	Udcpp + uBac \rightarrow UdcCjGlycan1 + UMP	Glover et al. (2006)
pglAHJ	GalNAc transferases	UdcCjGlycan1 + 5*UDP-GalNAc \rightarrow UdcCjGlycan6 + 5*UDP + 5*H ⁺	Glover et al. (2005)
pglI	Glucosyl transferase	UdcCjGlycan6 + UDP-Glc \rightarrow UdcCjGlycan + UDP + H ⁺	Kelly et al. (2006)
pglK	ATP-driven flippase	UdcCjGlycan + ATP + H ₂ O \rightarrow UdcCjGlycan(p) + ADP + H ⁺ + Pi	Kelly et al. (2006)
pglB	Oligosyltransferase	UdcCjGlycan(p) + AcceptorProt(p) \rightarrow GlycoProt + Udcppd(p)	Linton et al. (2005)

biosynthesis, we used heuristic optimization and the constraint-based model (see Materials and Methods). Coupling growth to glycan synthesis was desirable for several reasons. Foremost amongst these, growth-coupled strains create stoichiometric imbalances that reroute metabolic flux toward the desired product as a consequence of growth (Burgard et al., 2003; Feist et al., 2010). Therefore, faster growth requires increased glycan formation. Thus, optimizing glycan production through adaptive evolution is made trivial by selecting for growth through serial passage (Feist et al., 2010; Ibarra et al., 2002). Several methods have been developed to estimate genetic knockouts using constraint-based models. In this study, we used simulated annealing to search over the states of metabolic enzyme and transcription factor (TF) genes to identify the desired phenotype (Fig. 2). The state of each gene was represented as a binary array, where a one indicated normal activity, while a zero

indicated a genetic knockout or regulatory repression. Boolean rules informed by nutrient conditions controlled the TF genes, which in turn controlled the state of the metabolic genes. Once defined, the genetic state of the model modified the flux constraints placed on each reaction. For example, the reaction governed by pyruvate dehydrogenase, a multi-component enzyme, relied on the assembly of three enzymes: AceE, AceF, and Lpd. This reaction was encoded as:



Thus, if any of the genes *aceE*, *aceF*, or *lpd* was knocked out or transcriptionally repressed, the flux through this reaction was bound to zero. Gene-protein-reaction (GPR) associations from the iAF1260 network were used in this study (Feist et al., 2007). The simulated annealing algorithm performed a random search of genetic knockouts, iteratively

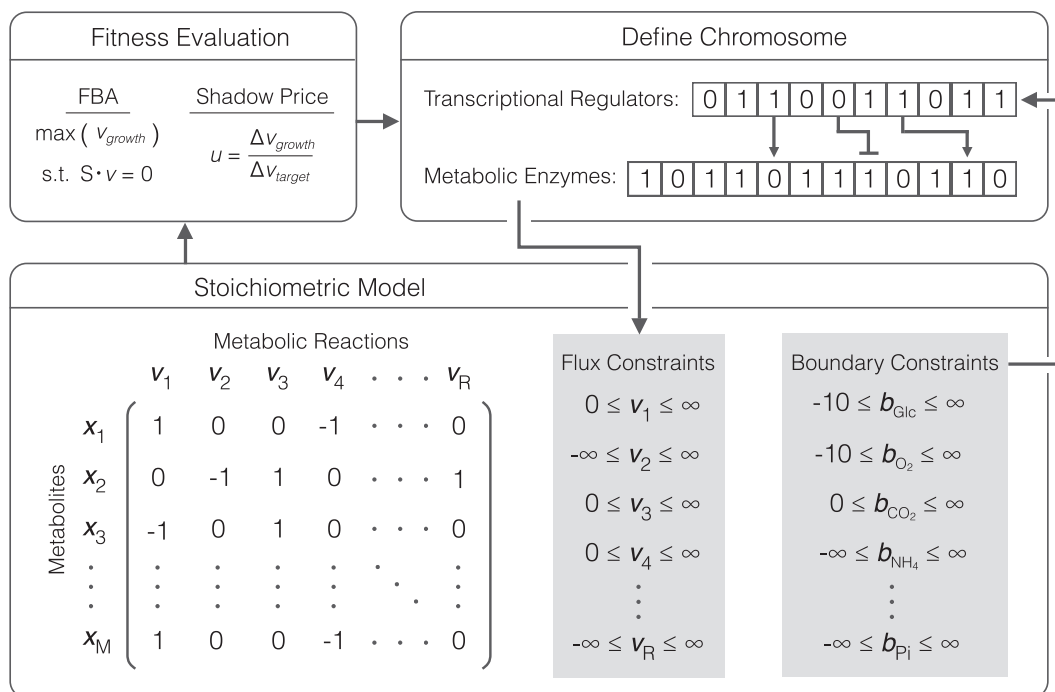


Fig. 2. Heuristic optimization approach used to identify strains coupling growth to glycan production. The chromosome is defined as two separate binary arrays, one defining the state of metabolic enzyme expression and another defining the state of transcriptional regulator activation. Gene repression and knockouts are designated by zeros. Nutrient conditions define the boundary constraints within the stoichiometric model which in turn affect the state of the metabolic enzyme chromosome. Gene repression and knockouts determine the constraints placed on fluxes in the stoichiometric model. Nutrients are mapped to the state of transcriptional regulators and genes are mapped to the state of flux constraints using Boolean rules as defined in (Feist et al., 2007; Covert et al., 2004). Flux balance analysis is used to maximize growth rate under the constraints imposed by the mutant strain and transcriptional regulation and the fitness objective is calculated. Here, we use shadow price; the strain is accepted or rejected based on the change in fitness and a Boltzmann criterion. New mutant strains are randomly generated from accepted ones. The search continues until a positive shadow price is achieved.

applying flux constraints based on the genetic state, then performing a flux balance analysis simulation. To identify growth-coupled glycan producing strains, we optimized the shadow price given by:

$$u_{\text{glycan}} = \frac{\Delta v_{\text{growth}}}{\Delta v_{\text{glycan}}} \quad (1)$$

where Δv_{growth} denotes the change in growth rate for a forced change in glycan flux Δv_{glycan} , and v_{glycan} denotes the flux representing the fully assembled *C. jejuni* glycan flipped into the periplasm. The shadow price u_{glycan} was calculated for a particular knockout strain by first calculating the optimal growth with the glycan flux constrained to zero. A second simulation was then performed with a forced incremental change in the glycan flux in order to obtain the difference in growth rate. The search algorithm continued until $u_{\text{glycan}} > 0$, indicating a growth-coupled phenotype (Supplementary Fig. S1).

We identified growth-coupled knockout strains with four or fewer knockouts for growth on glucose as the sole source of carbon and energy (Table 2). We performed optimization simulations using boundary conditions representing minimal medium with a single 6-, 5-, and 3-carbon substrate. A well-defined minimal media allowed for precise control over nutrient conditions experimentally, and was accurately simulated, particularly for the transcriptional regulatory network. For each substrate, we performed ten independent optimization simulations to identify growth-coupled strains. We considered growth-coupled strains with four or fewer knockouts (those most likely to be experimentally viable) by restricting the formation of extracellular byproducts to acetate. For example, for *E. coli* glycosylation mutant 2 (EcGM2; *E. coli* iAF1260 Δ sdh Δ gnd Δ pta Δ eutD), the strain with the highest simulated glycan yield, the optimal growth rate occurs at a non-zero glycan flux (Supplementary Fig. S1B). All growth-coupled strains contained a knockout of succinate dehydrogenase (*sdh*) and truncated pentose phosphate pathway (PPP) flux at either glucose 6-phosphate-1-dehydrogenase (*zwf*), 6-phosphogluconolactonase (*pgl*), or 6-phosphogluconate dehydrogenase (*gnd*).

2.3. Flux analysis of N-glycan production in growth-coupled strains

Growth-coupled glycan producing strains had increased glycolytic flux, and decreased amino acid biosynthesis compared to glycan production in the wt strain background (Fig. 3). We compared the normalized flux values for EcGM2 with the wt strain. Normalizing all fluxes to glucose uptake rate, EcGM2 displayed greater flux through glycolysis by cutting off the PPP via knockout of NADPH-producing *gnd* (Fig. 3A). EcGM2 also had decreased synthesis of every amino acid except for glutamine, indicating a source of stoichiometric imbalance that may be relieved by synthesis of the glycan precursor UDP-GlcNAc. Further, the PEP-pyruvate node acted as a switch point in central carbon metabolism (Fig. 3B). Here, PEP and pyruvate, the products of glycolysis, enter the TCA cycle through decarboxylation of pyruvate to acetyl-CoA (ACCoA) and carboxylation of PEP to form oxaloacetate (OAA) (Sauer and Eikmanns, 2005). The latter replenishes TCA cycle intermediates that exited TCA for anabolic processes. EcGM2, with a diminished anabolic capacity for cell growth, displayed lower flux through PEP carboxylase (*ppc*). However, as the result of high glycolytic flux, EcGM2 had increased flux

through pyruvate dehydrogenase (*aceEF*), sending carbon into the oxidative branch of the TCA cycle. It is known that high glucose uptake rates result in excess acetyl-CoA, surpassing the capacity of the TCA cycle. Because of this excess flux, wt *E. coli* grown on glucose commonly displays acetate fermentation, even under aerobic conditions (Gosset, 2005). We observed increased acetate secretion in EcGM1 simulations, but through a route differing from wild-type cells. The knockouts Δ pta and Δ eutD prevented ATP-generating acetate secretion. Flux was instead routed through the redox-neutral reactions initiated by acetaldehyde dehydrogenase (*mhpF*). Excess acetyl-CoA was also utilized in the pathway generating UDP-GlcNAc. Lastly, EcGM2 displayed a shift in cofactor production (Fig. 3C). Higher flux through glycolysis naturally led to NADH overproduction. On the other hand, the primary source of NADPH shifted from PPP genes *zwf* and *gnd* to the membrane transhydrogenase *pnt*, capable of direct transfer of electrons from NADH to NADP. Sauer et al. identified *pnt* as a major source of NADPH in *E. coli* (35–45% of total) (Sauer et al., 2004). Thus, *pnt* is capable of carrying significant flux *in vivo*. Taken together, these results suggested the model identified strains that promoted glycan precursor synthesis, primarily UDP-GlcNAc, by creating a combination of metabolite and redox imbalance.

2.4. Experimental validation of N-glycan-producing knockout strains

Glycan production was measured in the mutant strains to validate the model predictions (Fig. 4). Gene knockout strains were constructed using the Keio collection of single gene knockouts *E. coli* BW25113 (Baba et al., 2006) as donor strains for P1vir phage transduction. Mutants were constructed containing single, double, and triple knockouts that appeared in growth-coupled strains identified by the constraint-based model. We also performed simulations of each single gene knockout to determine genes that prevented glycan synthesis; *galU*, a key enzyme in the synthesis of glycan precursor UDP-glucose, was the only non-lethal knockout that prevented glycan synthesis. Knockout strains were transformed with a plasmid constitutively expressing the *C. jejuni* *pgl* locus. To quantify glycan production, we took advantage of crosstalk between the glycosylation pathway and native lipopolysaccharide (LPS) synthesis in *E. coli* (Hug and Feldman, 2011). Specifically, after the glycan is flipped into the periplasm, it can be transferred to lipid A-core by the WaaL O-antigen ligase and shuttled to the outer membrane by LPS pathway enzymes, where it is displayed on the cell surface (Merritt et al., 2013). Labeling of these surface-displayed N-glycans with fluorescently-tagged lectins can then be used to quantify the amount of glycan displayed on the cell surface as a measure of glycan production (Valderrama-Rincon et al., 2012). Here, we labeled *C. jejuni* glycans for detection by flow cytometry with fluorophore-conjugated soybean agglutinin (SBA), a lectin specific to terminal galactose and GalNAc residues. Prior to labeling, knockout strains were grown in glucose minimal media and harvested during the exponential growth phase, to most closely satisfy the pseudo-steady-state assumption of model predictions.

A common feature of the predicted mutant strains was the deletion of pentose phosphate pathway genes *zwf/pgl/gnd* in combination with Δ sdh. Analysis of the metabolic flux distribution in these mutants suggested the reducing state of the cell as well as the carbon flux was reprogrammed to

Table 2

Growth-coupled strains producing *C. jejuni* glycan identified by flux balance analysis and heuristic optimization using single carbon substrate. Knockouts listing multiple genes indicate that knockout of any one of those genes produces the same phenotype in the model. Abbreviations: D-Glucose, Glc; *E. coli* Wild type, EcWT; *E. coli* glycosylating mutant, EcGM.

Strain	Substrate	Genotype	Growth rate (/hr)	Glycan flux (mmol/gDW/hr)	Yield (mmol/gDW)
EcWT	Glucose	Wild type	0.78	0	0
EcGM1	Glucose	Δ sdh Δ (zwf/pgl/gnd)	0.65	0.012	0.018
EcGM2	Glucose	Δ sdh Δ (zwf/pgl/gnd) Δ pta Δ eutD	0.53	0.098	0.185
EcGM3	Glucose	Δ sdh Δ (zwf/pgl/gnd) Δ pykAF Δ mdh	0.64	0.016	0.025

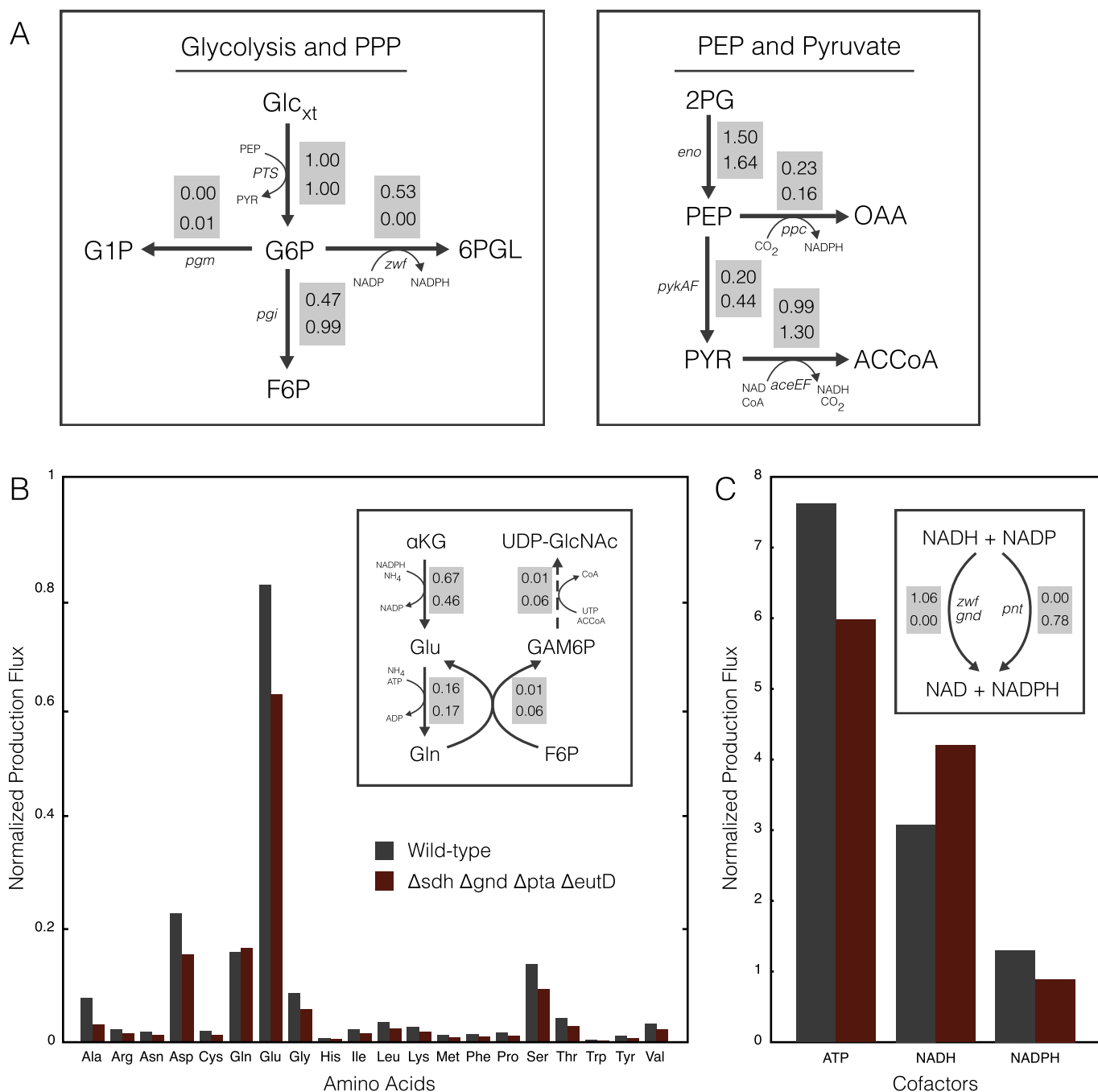


Fig. 3. Comparison of fluxes between the wild-type case and glycan-producing strain of type EcGM3 as calculated by flux balance analysis. **(A)** Fluxes through key nodes of metabolism. Top fluxes correspond to the wild-type case, bottom fluxes are for strain EcGM3. Fluxes are normalized by the glucose uptake rate. **(B)** Total flux into each amino acid, normalized to glucose uptake rate. Inset shows fluxes associated with glutamate and glutamine synthesis along with the pathway to glycan precursor UDP-GlcNAc. The dotted arrow represents a lumped pathway of multiple enzymes leading to the glycan precursor. **(C)** Total flux into selected cofactors, normalized to glucose uptake rate. Inset shows the primary modes of NADPH production in each strain. Abbreviations: Pentose phosphate pathway, PPP; Extracellular glucose, Glc_{xt}; Glucose-6-phosphate, G6P; Fructose 6-phosphate, F6P; 6-phospho D-glucono-1,5-lactone, 6PGL; Glucose 1-phosphate, G1P; Glycerate 2-phosphate, 2PG; Phosphoenolpyruvate, PEP; Pyruvate, PYR; Oxaloacetate, OAA; Acetyl-CoA, ACCoA; 2-Oxoglutarate, αKG; Glucosamine 6-phosphate, GAMP6P; UDP-N-acetyl-D-glucosamine, UDP-GlcNAc.

support enhanced glycan biosynthesis. While hypothetical knockouts such as Δsdh Δ(zwf/pgl/gnd) Δpta ΔeutD were predicted to have higher glycan yield, in this study we experimentally evaluated only the simplest growth-coupled double knockout family, namely EcGM1. The EcGM1 family had the largest predicted growth rate, was more experimentally tractable than the triple and quad knockouts, and was an unambiguous test of the reducing power hypothesis without the complication of the additional deletions. Thus, while the EcGM2 and EcGM3 families could

potentially give higher glycan flux, the EcGM1 family gave the clearest evaluation of the influence of the pentose phosphate pathway deletions. As predicted, single pentose phosphate knockouts Δzwf, Δpgl, and Δgnd displayed greater fluorescence than wt cells, with Δgnd being the most significant. However, when these deletions were combined with Δsdh only the Δsdh Δgnd combination led to increased glycan biosynthesis compared to wt cells. The single Δgnd mutant increased glycan production by nearly 3-fold compared to the wt strain background, while the

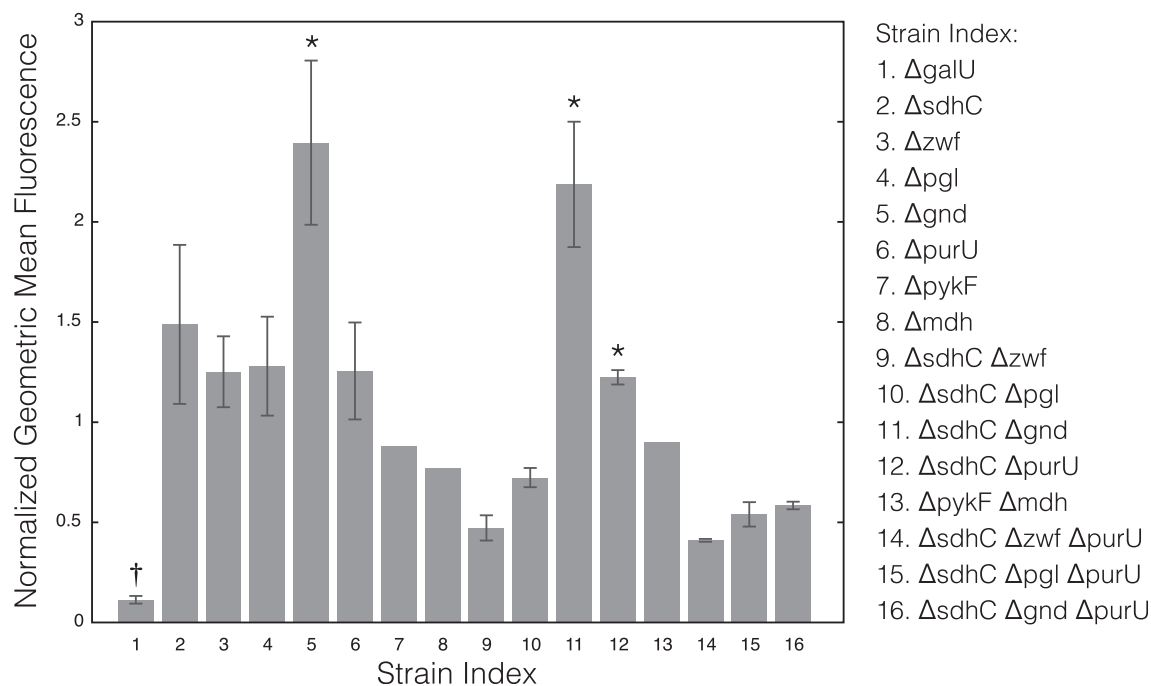


Fig. 4. Geometric mean fluorescence, normalized to the wild-type value, from gene knockout strains appearing in growth-coupled strains identified by the constraint-based model. † indicates a strain predicted to eliminate glycan flux. Stars indicate statistically significant increases in fluorescences according to a *t*-test ($p < 0.05$). Error bars indicate the standard deviation of at least three replicates.

$\Delta sdhC \Delta gnd$ combination led to a nearly 2.5-fold increase over the wt strain. Lastly, we tested the non-lethal deletions that were predicted to remove glycan biosynthesis; the $\Delta galU$ mutant showed no glycan production, thereby validating the model simulations. Taken together, constraint-based simulations predicted pentose phosphate pathway deletions in combination Δsdh (and potentially other genes) could improve glycan production by altering the redox state of the cell. We tested this hypothesis in the simplest possible experimental model, $\Delta sdh \Delta (zwf/pgl/gnd)$. Of the model predicted changes, only Δgnd alone and $\Delta sdhC \Delta gnd$ significantly increased glycan biosynthesis beyond the wt strain background. This suggested the model identified a potential axis for the improvement of glycan production, but results from the experimental system suggested this axis was likely more complicated as only the Δgnd and $\Delta sdhC \Delta gnd$ mutants gave a positive response.

3. Discussion

In this study we adapted a genome-scale model of *E. coli* metabolism for the simulation of heterologous synthesis of *N*-glycans. We applied heuristic optimization in combination with flux balance analysis to identify genetic knockouts that coupled *C. jejuni* glycan synthesis to growth. Simulations identified growth-coupled strains for minimal media growth on glucose as the sole source of carbon and energy. Flux analysis of these strains revealed two modes of flux redistribution that promoted glycan synthesis. For growth on glucose, simulations showed that maintaining high glycolytic flux and producing excess glutamine for the amination of glycan precursor sugars led to a growth-coupled phenotype. Simulations also identified the PPP as a primary target, suggesting the manipulation of the NADH/NADPH ratio influenced glycan synthesis. We validated model predictions by measuring cell surface-displayed *N*-glycans in *E. coli* mutants. In all growth conditions, the Δgnd mutant outperformed the wt strain in glycan synthesis. Overall, our model-guided strategy showed promise toward rationally designing a microbial glycosylation platform.

We used simulated annealing and flux balance analysis to search for metabolic and regulatory gene knockouts that produced a growth coupled phenotype. Several constraint-based methods have been

developed previously to identify gene knockouts that coupled production to growth e.g., (Burgard et al., 2003; Patil et al., 2005; Nair et al., 2017). Most of these methods rely on an OptKnock-like approach, whereby a bi-level mixed integer optimization problem is solved to identify the optimal set of gene knockouts. This class of method guarantees identification of the global optimum; however, it suffers from a few limitations. First, search time for OptKnock-like algorithms scales exponentially with system size and number of gene knockouts, making them unable to handle very large metabolic networks. Second, only linear engineering objectives (e.g., target production flux) can be searched over. In contrast, heuristic optimization is an effective approach for searching large networks while simultaneously considering non-linear objective functions. Though identification of the global optimum is not guaranteed with these methods, desirable sub-optimal solutions can be found quickly (Patil et al., 2005; Rocha et al., 2008). Also, heuristic optimization can search efficiently for gene knockouts rather than reaction knockouts. This is an important distinction because the mapping of genes to reactions is not necessarily one to one. Thus, experimentally, many reactions may be difficult to knock out because they may be catalyzed by the products of many genes. Here, we used simulated annealing in combination with flux balance analysis to maximize the shadow price of growth with respect to glycan flux using a genome scale metabolic reconstruction. The approach identified PPP knockouts that altered the NADH/NADPH balance, and increased glycolytic flux leading to enhanced glycan production. Surprisingly, these knockouts were not in the same section of the metabolism compared with previous literature studies. However, this may be expected, as we searched for growth coupled solutions and did not simply increase glycan formation. These solutions, while more difficult to obtain, offer a significant future advantage; namely, optimization of glycan production could be improved by selecting for increased growth through serial passage.

Often times, due to the simplifying assumptions of the model, the predicted mutant strains end up being difficult or impossible to construct in the lab. Also, it is not known *a priori* which combinations of knockouts will result in unviable strains. This does not make higher order knockout solutions unhelpful in achieving a metabolic engineering objective. More detailed flux analysis, like that in Fig. 3, of experimentally intractable

strains, might guide exploration of alternative genetic perturbations, such as knock-down and overexpression, that achieve a similar flux profile and resulting phenotype. Our approach, which allows for an unbiased random search of many potential knockout combinations at once, is able to identify suboptimal and/or higher order knockout strains that may be of great interest to experimentalists. Incorporation of alternative genomics datasets, such as 13C-based fluxomics measurements, would highlight metabolic pathways in least agreement with model predictions, thereby identifying potential alternative target perturbations. The interpretation and application of metabolic flux models by leveraging other information sources to overcome model deficiencies continues to be an exciting area of research.

Many aspects of glycoprotein production in *E. coli* are amenable to investigation and engineering by metabolic modeling. This study focused on increasing the availability of glycan precursor metabolites through model-guided metabolic network manipulations. Other approaches in bacteria have focused on optimizing expression of glycosylation pathway enzymes and identification of metabolic reaction targets through proteomic and genome engineering (Pandhal et al., 2011, 2012, 2013). Despite these efforts, improving glycosylation efficiency in *E. coli* remains a significant challenge. To address this challenge, a more comprehensive mathematical description of the cell, one that couples metabolism with gene expression and metabolic demand, may be required to precisely model glycosylation in *E. coli*. Our approach does not explicitly consider the metabolic burden associated with heterologous expression of glycosylation pathway enzymes nor the expression of the acceptor glycoprotein. Also, flux balance analysis lacks a description of enzyme kinetics and metabolite concentrations. Predicting phenotypic changes to genetic perturbations is a primary challenge in model-guided metabolic engineering (Link et al., 2014). It has been shown that single knockouts in the central metabolism of *E. coli* do little to change the relative flux distribution in the organism (Sauer et al., 1999). *E. coli* robustly controls metabolic flux using allosteric, transcriptional and post-transcriptional regulatory, and post-translational modification systems (Kremling et al., 2008; Link et al., 2013). Thus, glycoprotein production in *E. coli* is a unique challenge in that it requires optimization of two opposing cellular processes. Recombinant protein production of a desired glycoprotein along with glycosylation pathway enzymes requires energy from catabolic processes. On the other hand, glycan precursor synthesis requires conservation of available sugars and anabolic processes. The addition of regulatory systems and an explicit description of gene expression to a stoichiometric model may be an effective strategy for optimizing these opposing processes. Other strategies that may be helpful for optimization of this system include the enhancement of glycan precursor pathways, such as hexosamine synthesis, as well as the removal of competing pathways.

4. Materials and Methods

4.1. Flux balance analysis and heuristic optimization

Reactions encoding *C. jejuni* glycan formation (Table 1) were added to the genome-scale metabolic model of *E. coli* iAF1260 (Feist et al., 2007). The combined model was then used to determine growth coupled gene knockouts that improved glycan production flux. Metabolic fluxes were estimated using flux balance analysis. Flux balance analysis requires two assumptions. First, the cell was assumed to operate at a pseudo-steady-state, where the rate of production of every intracellular metabolite was equal to its consumption. Second, the cell has evolved to operate optimally to achieve a cellular objective. Though many objectives have been proposed, we use the most common, namely growth rate (i.e., biomass formation) maximization (Schuetz et al., 2007). The determination of a flux distribution satisfying these assumptions was formulated as a linear optimization problem:

$$\max_{\mathbf{v}} (v_{\text{growth}} = \mathbf{c}^T \mathbf{v})$$

Subject to : $\mathbf{S} \mathbf{v} = 0$

$$\alpha_i \leq v_i \leq \beta_i$$

where \mathbf{v} is the steady-state flux vector and α_i and β_i are the lower and upper limits for the individual flux values, respectively. The quantity, v_{growth} , denotes the specific growth rate where \mathbf{c} is a vector containing the stoichiometric contribution of each metabolic species to biomass. The stoichiometric matrix \mathbf{S} encodes all biochemical reaction connectivity considered in the model. Each row of \mathbf{S} describes a metabolite, while each column describes a particular reaction. The (i, j) element of \mathbf{S} , denoted by σ_{ij} , describes how species i participates in reaction j . If $\sigma_{ij} > 0$, species i is produced by reaction j . Conversely, if $\sigma_{ij} < 0$, then species i is consumed by reaction j . Lastly, if $\sigma_{ij} = 0$, then species i is not involved in reaction j . The maximum substrate and oxygen uptake rates were set at 10 mmol/gDW/hr. Boundary conditions were set to allow for the unrestricted formation of acetate. All genes found to be essential for growth on Luria-Bertani (LB) medium were excluded from the search (Baba et al., 2006).

We used the FastPros algorithm developed by Ohno et al., in combination with a shadow price objective, to estimate genetic knockouts (Ohno et al., 2014). Simulated annealing identified growth-coupled genetic knockouts with improved glycan production (Kirkpatrick et al., 1983). Prior to optimization, we removed all genes associated with dead end reactions, since knocking those out would have no effect on the network. Also, we removed duplicate genes, i.e., those that produced identical effects when knocked out. Finally, we removed genes whose knockout resulted in zero growth. We searched over both metabolic and regulatory genes; metabolic and transcriptional regulatory genes were represented by a binary array where 1 indicated the gene was expressed, and 0 zero indicated it was removed from the network (or transcriptionally repressed). A random initial gene knockout array was generated. We allowed for a maximum of 20 knockouts during the search. At each iteration, a new knockout array was generated through mutation operations that randomly introduced new knockouts and rearranged existing knockouts similar to (Patil et al., 2005). Briefly, new knockouts were introduced for each gene with probability $\mathcal{P}(\text{mutate}) = 10^{-4}$. If necessary, knockouts were randomly removed to limit their total number to 20. Then, a random number of knockouts were rearranged (i.e., removed from one gene and assigned to another). At each iteration, the fitness (shadow price) of an individual was computed using flux balance analysis. When an individual with a higher fitness was encountered (greater shadow price), that individual was accepted. However, when an individual with a lower fitness was encountered, we accepted this individual with a probability given by a Boltzmann factor:

$$\mathcal{P}(\text{accept}) = e^{-\Delta u_{\text{glycan}}/T} \quad (2)$$

where Δu_{glycan} denotes the change in shadow price between the current and previous solution, and the temperature T denotes the computational annealing temperature which decreased with the search iteration. The annealing temperature T decreased exponentially such that $T_{k+1} = \alpha T_k$, where k denotes the iteration index and α denotes the cooling rate defined as (Rocha et al., 2008):

$$\alpha = \exp\left(\frac{\log T_f - \log T_o}{N_{\text{max}}/N_\alpha}\right) \quad (3)$$

The term N_{max} denotes the maximum allowable number of objective function evaluations ($N_{\text{max}} = 10,000$), and N_α denotes the number of objective function evaluations performed at each distinct temperature value ($N_\alpha = 1$). The initial temperature T_o was defined as $T_o = -\frac{\Delta u_{\text{glycan},o}}{\log 0.5}$, while the final temperature T_f was given by $T_f = -\frac{\Delta u_{\text{glycan},f}}{\log 0.5}$. Lastly, $\Delta u_{\text{glycan},o}$ denotes the difference in shadow price corresponding to an acceptance probability of worse solutions of 50% at the beginning of the search, and $\Delta u_{\text{glycan},f}$ is the shadow price difference giving a 50%

probability of accepting a worse solution by the end of the search. These values were approximated using the typical shadow price values of random knockout arrays: $\Delta u_{glycan,o} = 0.005$, $\Delta u_{glycan,f} = 0.0005$.

Though we sought to maximize glycan flux, we also wanted to identify experimentally viable strains. Thus, during an optimization search, we set a lower bound on the biomass reaction flux equal to 10% of the wild-type simulated growth rate. Strains that could not meet this constraint were ignored. The knockout search was terminated once a positive shadow price was found. After the optimization, we processed growth-coupled knockout strains by iteratively knocking in each knockout gene to estimate knockouts that did not affect the phenotype. In this way we identified the smallest number of gene knockouts that produced enhanced glycan flux at optimal growth. Each optimization run required approximately 6 h on a single CPU Apple workstation (Apple, Cupertino, CA, USA; OS X v10.10). All model and optimization code is available in the MATLAB (The Mathworks, Natick MA) programming language, and free to download under an MIT software license from Varnerlab.org (<http://www.varnerlab.org/>).

4.2. Bacterial strains and media

For surface-labeled glycan fluorescence measurements, we used the *E. coli* strain BW25113 as our wild-type case (Baba et al., 2006). BW25113 was used as the parent strain to construct all gene knockout strains. Plasmid pCP20 was used to excise KmR cassette (Cherepanov and Wackernagel, 1995). Minimal media consisted of 33.9 g/L Na_2HPO_4 , 15.0 g/L KH_2PO_4 , 5.0 g/L NH_4Cl , and 2.5 g/L NaCl. Media was supplemented with 0.4% glucose. Growth medium was supplemented by appropriate antibiotic at: 100 $\mu\text{g}/\text{mL}$ ampicillin (Amp), 25 $\mu\text{g}/\text{mL}$ chloramphenicol, and 50 $\mu\text{g}/\text{mL}$ kanamycin (Kan). Growth was monitored by measuring optical density at 600 nm (OD_{600}).

4.3. Flow cytometry

BW25113-based knockout strains were transformed with plasmid pACYCpgl, constitutively expressed by the *C. jejuni* *pgl* locus. Cultures were inoculated from frozen stock in LB and grew for 3–6 h. Cells were subcultured 1:100 in minimal media overnight and then transferred to fresh minimal media to an OD_{600} of 0.1. 300 μL cells were harvested during exponential growth phase ($\text{OD}_{600} \approx 0.6$). Cells were washed with PBS then incubated in the dark for 15 min at 37 °C. Cells were resuspended in 5 $\mu\text{g}/\text{mL}$ SBA-Alexa Fluor 488 (Invitrogen) and 500 μL PBS and analyzed using a FACSCalibur (Becton Dickinson). Geometric mean fluorescence was determined from 100,000 events.

Author contributions

J.V and M.P.D directed the study. J.W constructed the mathematical model and conducted the computational studies. T.M, C.G and J.W created the mutant strains and conducted the experimental studies. The manuscript was prepared and edited for publication by J.V, M.P.D, T.M and J.W. All authors reviewed the manuscript.

Conflicts of interest

M.P.D has a financial interest in Glycobia, Inc. J.V, T.M, C.G and J.W have no competing financial interests.

Funding

This study was supported by an award from the National Science Foundation (MCB-1411715) to M.D and J.V and by an award from the US Army (Systems Biology of Trauma Induced Coagulopathy W911NF-10-1-0376) to J.V. for the support of J.W.

Appendix A. Supplementary data

Supplementary data to this article can be found online at <https://doi.org/10.1016/j.mec.2019.e00088>.

References

- Baba, T., Ara, T., Hasegawa, M., Takai, Y., Okumura, Y., Baba, M., Datsenko, K.A., Tomita, M., Wanner, B.L., Mori, H., 2006. Construction of escherichia coli k-12 in-frame, single-gene knockout mutants: the keio collection. *Mol. Syst. Biol.* 2, 2006.0008.
- Baker, J.L., Çelik, E., DeLisa, M.P., 2013. Expanding the glycoengineering toolbox: the rise of bacterial n-linked protein glycosylation. *Trends Biotechnol.* 31, 313–323.
- Bernatchez, S., Szymanski, C.M., Ishiyama, N., Li, J., Jarrell, H.C., Lau, P.C., Berghuis, A.M., Young, N.M., Wakarchuk, W.W., 2005. A single bifunctional udp-glcnac/glc 4-epimerase supports the synthesis of three cell surface glycoconjugates in campylobacter jejuni. *J. Biol. Chem.* 280, 4792–4802.
- Burgard, A.P., Pharkya, P., Maranas, C.D., 2003. OptKnock: a bilevel programming framework for identifying gene knockout strategies for microbial strain optimization. *Biotechnol. Bioeng.* 84, 647–657.
- Cherepanov, P.P., Wackernagel, W., 1995. Gene disruption in escherichia coli: Tcr and kmr cassettes with the option of flip-catalyzed excision of the antibiotic-resistance determinant. *Gene* 158, 9–14.
- Covert, M.W., Knight, E.M., Reed, J.L., Herrgard, M.J., Palsson, B.O., 2004. Integrating high-throughput and computational data elucidates bacterial networks. *Nature* 429, 92–96.
- Dell, A., Galadari, A., Sastre, F., Hitchen, P., 2010. Similarities and differences in the glycosylation mechanisms in prokaryotes and eukaryotes. *Internet J. Microbiol.* 2010, 148178.
- Elliott, S., Lorenzini, T., Asher, S., Aoki, K., Brankow, D., Buck, L., Busse, L., Chang, D., Fuller, J., Grant, J., Hernday, N., Hokum, M., Hu, S., Knudten, A., Levin, N., Komorowski, R., Martin, F., Navarro, R., Osslund, T., Rogers, G., Rogers, N., Trail, G., Egrie, J., 2003. Enhancement of therapeutic protein in vivo activities through glycoengineering. *Nat. Biotechnol.* 21, 414–421.
- Feist, A.M., Henry, C.S., Reed, J.L., Krummenacker, M., Joyce, A.R., Karp, P.D., Broadbelt, L.J., Hatzimanikatis, V., Palsson, B.O., 2007. A genome-scale metabolic reconstruction for escherichia coli k-12 mg1655 that accounts for 1260 orfs and thermodynamic information. *Mol. Syst. Biol.* 3, 121.
- Feist, A.M., Zielinski, D.C., Orth, J.D., Schellenberger, J., Herrgard, M.J., Palsson, B.O., 2010. Model-driven evaluation of the production potential for growth-coupled products of escherichia coli. *Metab. Eng.* 12, 173–186.
- Feldman, M.F., Wacker, M., Hernandez, M., Hitchen, P.G., Marolda, C.L., Kowarik, M., Morris, H.R., Dell, A., Valvano, M.A., Aebi, M., 2005. Engineering n-linked protein glycosylation with diverse o antigen lipopolysaccharide structures in escherichia coli. *Proc. Natl. Acad. Sci. U. S. A.* 102, 3016–3021.
- Fisher, A.C., Haitjema, C.H., Guarino, C., Çelik, E., Endicott, C.E., Reading, C.A., Merritt, J.H., Ptak, A.C., Zhang, S., DeLisa, M.P., 2011. Production of secretory and extracellular n-linked glycoproteins in escherichia coli. *Appl. Environ. Microbiol.* 77, 871–881.
- Flintegaard, T.V., Thygesen, P., Rahbek-Nielsen, H., Levery, S.B., Kristensen, C., Clausen, H., Bolt, G., 2010. N-glycosylation increases the circulatory half-life of human growth hormone. *Endocrinology* 151, 5326–5336.
- Glover, K.J., Weerapana, E., Imperiali, B., 2005. In vitro assembly of the undecaprenylpyrophosphate-linked heptasaccharide for prokaryotic n-linked glycosylation. *Proc. Natl. Acad. Sci. U. S. A.* 102, 14255–14259.
- Glover, K.J., Weerapana, E., Chen, M.M., Imperiali, B., 2006. Direct biochemical evidence for the utilization of udp-bacillosamine by *pglc*, an essential glycosyl-1-phosphate transferase in the campylobacter jejuni n-linked glycosylation pathway. *Biochemistry* 45, 5343–5350.
- Gosset, G., 2005. Improvement of escherichia coli production strains by modification of the phosphoenolpyruvate:sugar phosphotransferase system. *Microb. Cell Factories* 4, 14. <http://www.varnerlab.org/downloads/???>
- Hug, I., Feldman, M.F., 2011. Analogies and homologies in lipopolysaccharide and glycoprotein biosynthesis in bacteria. *Glycobiology* 21, 138–151.
- Ibarra, R.U., Edwards, J.S., Palsson, B.O., 2002. Escherichia coli k-12 undergoes adaptive evolution to achieve in silico predicted optimal growth. *Nature* 420, 186–189.
- Ihsen, J., Kowarik, M., Diletto, S., Tanner, C., Wacker, M., Thöny-Meyer, L., 2010. Production of glycoprotein vaccines in escherichia coli. *Microb. Cell Factories* 9, 61.
- Ilyushin, D.G., Smirnov, I.V., Belogurov Jr., A.A., Dyachenko, I.A., Zharmukhamedova, T.I., Novozhilova, T.I., Bychikhin, E.A., Serebryakova, M.V., Kharybin, O.N., Murashev, A.N., Anikienko, K.A., Nikolaev, E.N., Ponomarenko, N.A., Genkin, D.D., Blackburn, G.M., Masson, P., Gabibov, A.G., 2013. Chemical polysialylation of human recombinant butyrylcholinesterase delivers a long-acting bioscavenger for nerve agents in vivo. *Proc. Natl. Acad. Sci. U. S. A.* 110, 1243–1248.
- Jaffé, S.R., Stratton, B., Levarski, Z., Pandhal, J., Wright, P.C., 2014. Escherichia coli as a glycoprotein production host: recent developments and challenges. *Curr. Opin. Biotechnol.* 30C, 205–210.
- Kämpf, M.M., Braun, M., Sirena, D., Ihsen, J., Thöny-Meyer, L., Ren, Q., 2015. In vivo production of a novel glycoconjugate vaccine against shigella flexneri 2a in recombinant escherichia coli: identification of stimulating factors for in vivo glycosylation. *Microb. Cell Factories* 14, 12.
- Kelly, J., Jarrell, H., Millar, L., Tessier, L., Fiori, L.M., Lau, P.C., Allan, B., Szymanski, C.M., 2006. Biosynthesis of the n-linked glycan in campylobacter jejuni and addition onto protein through block transfer. *J. Bacteriol.* 188, 2427–2434.

- Kirkpatrick, S., Gelatt Jr., C.D., Vecchi, M.P., 1983. Optimization by simulated annealing. *Science* 220, 671–680.
- Kowarik, M., Young, N.M., Numao, S., Schulz, B.L., Hug, I., Callewaert, N., Mills, D.C., Watson, D.C., Hernandez, M., Kelly, J.F., Wacker, M., Aebi, M., 2006. Definition of the bacterial n-glycosylation site consensus sequence. *EMBO J.* 25, 1957–1966.
- Kremling, A., Bettenbrock, K., Gilles, E.D., 2008. A feed-forward loop guarantees robust behavior in *Escherichia coli* carbohydrate uptake. *Bioinformatics* 24, 704–710.
- Li, T., DiLillo, D.J., Bournazos, S., Giddens, J.P., Ravetch, J.V., Wang, L.-X., 2017. Modulating IgG effector function by Fc glycan engineering. *Proc. Natl. Acad. Sci. U. S. A.* 114, 3485–3490.
- Lin, C.-W., Tsai, M.-H., Li, S.-T., Tsai, T.-I., Chu, K.-C., Liu, Y.-C., Lai, M.-Y., Wu, C.-Y., Tseng, Y.-C., Shivatare, S.S., Wang, C.-H., Chao, P., Wang, S.-Y., Shih, H.-W., Zeng, Y.-F., You, T.-H., Liao, J.-Y., Tu, Y.-C., Lin, Y.-S., Chuang, H.-Y., Chen, C.-L., Tsai, C.-S., Huang, C.-C., Lin, N.-H., Ma, C., Wu, C.-Y., Wong, C.-H., 2015. A common glycan structure on immunoglobulin G for enhancement of effector functions. *Proc. Natl. Acad. Sci. U. S. A.* 112, 10611–10616.
- Lindhout, T., Iqbal, U., Willis, L.M., Reid, A.N., Li, J., Liu, X., Moreno, M., Wakarchuk, W.W., 2011. Site-specific enzymatic polysialylation of therapeutic proteins using bacterial enzymes. *Proc. Natl. Acad. Sci. U. S. A.* 108, 7397–7402.
- Link, H., Kochanowski, K., Sauer, U., 2013. Systematic identification of allosteric protein-metabolite interactions that control enzyme activity in vivo. *Nat. Biotechnol.* 31, 357–361.
- Link, H., Christodoulou, D., Sauer, U., 2014. Advancing metabolic models with kinetic information. *Curr. Opin. Biotechnol.* 29C, 8–14.
- Linton, D., Dorrell, N., Hitchen, P.G., Amber, S., Karlyshev, A.V., Morris, H.R., Dell, A., Valvano, M.A., Aebi, M., Wren, B.W., 2005. Functional analysis of the campylobacter jejuni n-linked protein glycosylation pathway. *Mol. Microbiol.* 55, 1695–1703.
- Lipinski, T., Fiteh, A., St Pierre, J., Ostergaard, H.L., Bundle, D.R., Touret, N., 2013. Enhanced immunogenicity of a tricomponent mannan tetanus toxoid conjugate vaccine targeted to dendritic cells via dectin-1 by incorporating β -glucan. *J. Immunol.* 190, 4116–4128.
- Merritt, J.H., Ollis, A.A., Fisher, A.C., DeLisa, M.P., 2013. Glycans-by-design: engineering bacteria for the biosynthesis of complex glycans and glycoconjugates. *Biotechnol. Bioeng.* 110, 1550–1564.
- Nair, G., Jungreuthmayer, C., Zanghellini, J., 2017. Optimal knockout strategies in genome-scale metabolic networks using particle swarm optimization. *BMC Bioinf.* 18, 78.
- Nothaft, H., Szymanski, C.M., 2010. Protein glycosylation in bacteria: sweeter than ever. *Nat. Rev. Microbiol.* 8, 765–778.
- Ohno, S., Shimizu, H., Furusawa, C., 2014. Fastpros: screening of reaction knockout strategies for metabolic engineering. *Bioinformatics* 30, 981–987.
- Olivier, N.B., Chen, M.M., Behr, J.R., Imperiali, B., 2006. In vitro biosynthesis of udp-n,n'-diacetyl bacillosamine by enzymes of the campylobacter jejuni general protein glycosylation system. *Biochemistry* 45, 13659–13669.
- Pandhal, J., Ow, S.Y., Noirel, J., Wright, P.C., 2011. Improving n-glycosylation efficiency in *Escherichia coli* using shotgun proteomics, metabolic network analysis, and selective reaction monitoring. *Biotechnol. Bioeng.* 108, 902–912.
- Pandhal, J., Desai, P., Walpole, C., Doroudi, L., Malyshev, D., Wright, P.C., 2012. Systematic metabolic engineering for improvement of glycosylation efficiency in *Escherichia coli*. *Biochem. Biophys. Res. Commun.* 419, 472–476.
- Pandhal, J., Woodruff, L.B.A., Jaffe, S., Desai, P., Ow, S.Y., Noirel, J., Gill, R.T., Wright, P.C., 2013. Inverse metabolic engineering to improve *Escherichia coli* as an n-glycosylation host. *Biotechnol. Bioeng.* 110, 2482–2493.
- Patil, K.R., Rocha, I., Förster, J., Nielsen, J., 2005. Evolutionary programming as a platform for in silico metabolic engineering. *BMC Bioinf.* 6, 308.
- Rocha, M., Maia, P., Mendes, R., Pinto, J.P., Ferreira, E.C., Nielsen, J., Patil, K.R., Rocha, I., 2008. Natural computation meta-heuristics for the in silico optimization of microbial strains. *BMC Bioinf.* 9, 499.
- Sadoulet, M.-O., Franceschi, C., Aubert, M., Silvy, F., Bernard, J.-P., Lombardo, D., Mas, E., 2007. Glycoengineering of alphaGal xenoantigen on recombinant peptide bearing the j28 pancreatic oncofetal glycotope. *Glycobiology* 17, 620–630.
- Sauer, U., Eikmanns, B.J., 2005. The pep-pyruvate-oxaloacetate node as the switch point for carbon flux distribution in bacteria. *FEMS Microbiol. Rev.* 29, 765–794.
- Sauer, U., Lasko, D.R., Fiaux, J., Hochuli, M., Glaser, R., Szyperski, T., Wüthrich, K., Bailey, J.E., 1999. Metabolic flux ratio analysis of genetic and environmental modulations of *Escherichia coli* central carbon metabolism. *J. Bacteriol.* 181, 6679–6688.
- Sauer, U., Canonaco, F., Heri, S., Perrenoud, A., Fischer, E., 2004. The soluble and membrane-bound transhydrogenases *udha* and *pnab* have divergent functions in nadph metabolism of *Escherichia coli*. *J. Biol. Chem.* 279, 6613–6619.
- Schoenhofen, I.C., McNally, D.J., Vinogradov, E., Whitfield, D., Young, N.M., Dick, S., Wakarchuk, W.W., Brisson, J.-R., Logan, S.M., 2006. Functional characterization of dehydratase/aminotransferase pairs from *Helicobacter* and *Campylobacter*: enzymes distinguishing the pseudaminic acid and bacillosamine biosynthetic pathways. *J. Biol. Chem.* 281, 723–732.
- Schuetz, R., Kuepfer, L., Sauer, U., 2007. Systematic evaluation of objective functions for predicting intracellular fluxes in *Escherichia coli*. *Mol. Syst. Biol.* 3, 119.
- Schwarz, F., Huang, W., Li, C., Schulz, B.L., Lizak, C., Palumbo, A., Numao, S., Neri, D., Aebi, M., Wang, L.-X., 2010. A combined method for producing homogeneous glycoproteins with eukaryotic n-glycosylation. *Nat. Chem. Biol.* 6, 264–266.
- Szymanski, C.M., Yao, R., Ewing, C.P., Trust, T.J., Guerry, P., 1999. Evidence for a system of general protein glycosylation in *Campylobacter jejuni*. *Mol. Microbiol.* 32, 1022–1030.
- Valderrama-Rincon, J.D., Fisher, A.C., Merritt, J.H., Fan, Y.-Y., Reading, C.A., Chhiba, K., Heiss, C., Azadi, P., Aebi, M., DeLisa, M.P., 2012. An engineered eukaryotic protein glycosylation pathway in *Escherichia coli*. *Nat. Chem. Biol.* 8, 434–436.
- Wacker, M., Linton, D., Hitchen, P.G., Nita-Lazar, M., Haslam, S.M., North, S.J., Panico, M., Morris, H.R., Dell, A., Wren, B.W., Aebi, M., 2002. N-linked glycosylation in *Campylobacter jejuni* and its functional transfer into *E. coli*. *Science* 298, 1790–1793.
- Wacker, M., Wang, L., Kowarik, M., Dowd, M., Lipowsky, G., Faridmoayer, A., Shields, K., Park, S., Alaimo, C., Kelley, K.A., Braun, M., Quebatte, J., Gambillara, V., Carranza, P., Steffen, M., Lee, J.C., 2014. Prevention of *Staphylococcus aureus* infections by glycoprotein vaccines synthesized in *Escherichia coli*. *J. Infect. Dis.* 209, 1551–1561.